

# 2610 Spatiotemporal maps for dynamic MRI reconstruction: a proof-of-principle demonstration on single-coil animal gastrointestinal data

Rodrigo A. Lobos<sup>1</sup>, Xiaokai Wang<sup>1</sup>, Zhongming Liu<sup>1</sup>, Jeffrey A. Fessler<sup>2</sup>, and Douglas C. Noll<sup>1</sup>

<sup>1</sup>Biomedical Engineering, University of Michigan, Ann Arbor, MI, United States, <sup>2</sup>Electrical and Computer Engineering, University of Michigan, Ann Arbor, MI, United States

## Synopsis

**Keywords:** Image Reconstruction, Image Reconstruction, Dynamic MRI reconstruction

**Motivation:** Partially separable functions (PSF) are commonly used in dynamic MRI to model the signal in the (x,t)-space; however, the number of components in the PSF expansion can be restrictive in applications where voxels present different temporal/spectral characteristics (e.g., gastrointestinal MRI reconstruction).

**Goal(s):** To propose a parsimonious representation for the dynamic MRI signal, called spatiotemporal maps (STM).

**Approach:** STM are derived by proving that shift-invariant linear predictability relationships can exist across the k-spaces of multiple time-frames.

**Results:** STM provide a parsimonious representation for the spatiotemporal MRI signal; they can be efficiently calculated from autocalibration data; and they can be synergistically combined with modern regularizers.

**Impact:** Spatiotemporal maps provide a parsimonious voxel-dependent expansion for the dynamic MRI signal, even when voxels present various temporal/spectral characteristics. They can be efficiently calculated from autocalibration data, and can be synergistically combined with modern regularizers to reconstruct highly accelerated data.

## Introduction

Partially separable functions<sup>1</sup> (PSF) have been widely used in dynamic MRI reconstruction to describe the spatiotemporal MRI signal<sup>2-5</sup>. The PSF model assumes that each voxel of the spatiotemporal signal can be expanded as a sum of products, each one involving a spatial function (voxel-dependent) and a temporal function (voxel-independent). Nevertheless, the number of components in the PSF expansion can be undesirably large in applications where voxels present different temporal/spectral properties and limited data is available<sup>1</sup>. In this work we account for these limitations by proposing a more parsimonious expansion than PSF, that we call spatiotemporal maps (STM). In the STM expansion each component corresponds to a product between a spatial function, that is voxel-dependent, and a spatiotemporal function that is also voxel-dependent. Thus, the temporal dynamics in the STM expansion are captured for each voxel separately, which provides them with powerful parsimonious representation capabilities. We show that STM can be synergistically combined with modern regularizers to reconstruct highly accelerated data where, in addition, temporal/spectral characteristics vary substantially across voxels. As a proof-of-principle, we address the reconstruction of single-coil animal gastrointestinal data<sup>6,7</sup>.

## Theory

Let  $q(\mathbf{x}, n\Delta t)$ ,  $n \in \{1, \dots, N\}$  denote the spatiotemporal MRI signal sampled in time. The derivation of the STM expansion is based on proving the existence of multiple shift-invariant linear predictability (SILP) relationships<sup>8</sup> across the k-space samples of multiple time-frames. We have theoretically shown that if  $q(\mathbf{x}, t)$  has a voxel-dependent limited spectral support over multiple bands, then the desired SILP relationships exist (the full proof is not shown due to space constraints). According to recent work in sensitivity map estimation<sup>9</sup>, SILP across time-frames would suggest that, if we consider the k-space data of each time-frame as a virtual channel, we would be able to derive a signal model analogous to sensitivity maps. In fact, SILP implies that we can construct voxel-dependent positive semidefinite matrices  $\mathbf{G}(\mathbf{x}) \in \mathbb{C}^{N \times N}$  from (k,t)-space autocalibration data<sup>9</sup>, that satisfy

$$\mathbf{G}(\mathbf{x}) \begin{bmatrix} q(\mathbf{x}, 1\Delta t) \\ \vdots \\ q(\mathbf{x}, N\Delta t) \end{bmatrix} \approx \mathbf{0}.$$

This reveals that the spatiotemporal MRI signal for one specific voxel is an approximate nullspace vector of the corresponding matrix  $\mathbf{G}(\mathbf{x})$ . We construct the STM expansion by calculating a basis for the nullspace of each matrix  $\mathbf{G}(\mathbf{x})$ , where the number of components  $L(\mathbf{x})$  is the nullspace dimensionality. The STM expansion has the form

$$q(\mathbf{x}, n\Delta t) \approx \sum_{l=1}^{L(\mathbf{x})} c_l(\mathbf{x}, n\Delta t) \underline{q}_l(\mathbf{x}), \quad n \in \{1, \dots, N\},$$

where  $c_l(\mathbf{x}, n\Delta t)$  and  $\underline{q}_l(\mathbf{x})$  correspond to the voxel-dependent spatiotemporal function and the spatial function of the  $l$ th component, respectively. The spatiotemporal functions for one specific voxel (i.e.,  $\{c_l(\mathbf{x}, n\Delta t)\}$ ) correspond to a basis for the nullspace of  $\mathbf{G}(\mathbf{x})$ ; they can be efficiently calculated from autocalibration data<sup>9</sup>, and used as a data-consistency constraint in reconstruction applications. We pose the reconstruction problem such that the spatial functions (i.e.,  $\{\underline{q}_l(\mathbf{x})\}$ ) correspond to the optimization variables, as the number of components in the STM expansion is usually much smaller than the number of time-frames. We impose complementary constraints over  $\{\underline{q}_l(\mathbf{x})\}$  using application-dependent regularizers, and we recover the reconstructed time-series using the last equation.

## Methods

STM were assessed by reconstructing single-coil animal gastrointestinal Cartesian data<sup>6,7</sup> (Fig. 1) that was retrospectively and uniformly undersampled ( $R = 3.5$ ) outside an autocalibration region. We also reconstructed a prospectively undersampled dataset ( $R = 2$ ) acquired as in Wang et al<sup>6</sup>. Both reconstructions were performed in blocks of  $N = 25$  time-frames. STM spatiotemporal functions were estimated from autocalibration data using PISCO<sup>9</sup>, and we investigated the combination of STM with Tikhonov and P-LORAKS<sup>11</sup> regularizers using an iterative least-squares reconstruction approach.

## Results

Figure 2 shows the eigenvalue maps of the matrices  $\mathbf{G}(\mathbf{x})$  for the data in Fig. 1. From these we selected  $L(\mathbf{x}) = L = 3$ , after identifying the number of eigenvalues below a threshold of 0.01. Figure 1 shows the different functions in the STM expansion. Figure 3 compares STM and PSF where the normalized projection residual<sup>9,10</sup> was calculated for different numbers of components. STM obtained considerably smaller values than PSF when the number of components was small, which quantitatively indicates better representation capabilities. Figures 4 and 5 show the retrospective and prospective reconstruction results, respectively. STM with P-LORAKS regularization obtained the best quantitative results (smallest NRMSE), and a considerable qualitative improvement over previously proposed reconstruction methods<sup>6,7</sup>.

## Discussion and Conclusions

The STM expansion can represent dynamic MRI signals more parsimoniously than PSF in scenarios where voxels present substantially varying temporal/spectral characteristics. STM can be efficiently calculated from autocalibration data, and synergistically combined with modern regularizers to reconstruct highly accelerated data. Future work involves combining STM with parallel imaging constraints, non-Cartesian acquisition, and data-driven regularizers.

## Acknowledgements

This work was supported by the National Institutes of Health through grants R21EB034344 and R01AT011665.

## References

- [1] Liang ZP. "Spatiotemporal imaging with partially separable functions". *2007 4th IEEE International Symposium on Biomedical Imaging: From Nano to Macro*. pp. 988-991, 2007.
- [2] Haldar JP, Liang ZP. "Spatiotemporal imaging with partially separable functions: A matrix recovery approach". *2010 IEEE International Symposium on Biomedical Imaging: From Nano to Macro*. pp. 716-719, 2007.
- [3] Zhao B, Haldar JP, Christodoulou AG, Liang ZP. "Image reconstruction from highly undersampled (k, t)-space data with joint partial separability and sparsity constraints". *IEEE Transactions on Medical Imaging*. 31(9):1809-1820, 2012.
- [4] Lingala SG, Hu Y, DiBella E, Jacob M. "Accelerated dynamic MRI exploiting sparsity and low-rank structure: k-t SLR". *IEEE Transactions on Medical Imaging*, 30(5), 1042-1054, 2011.
- [5] Jin R, Li Y, Shosted RK, Xing F, Gilbert I, Perry JL, Woo J, Liang ZP, Sutton BP. "Optimization of 3D dynamic speech MRI: Poisson-disc undersampling and locally higher-rank reconstruction through partial separability model with regional optimized temporal basis". *Magnetic Resonance in Medicine*, 91(1): 61-74, 2024.
- [6] Wang X, Cao J, Han K, Choi M, She Y, Scheven UM, Avci R, Du P, Cheng LK, Di Natale MR, Furness JB, Liu Z. "Diffeomorphic surface modeling for MRI-based characterization of gastric anatomy and motility". *IEEE Transactions on Biomedical Engineering*. 70(7):2046-57, 2023.
- [7] Wang X, Alkaabi F, Choi M, Di Natale MR, Scheven UM, Noll DC, Furness JB, Liu Z. "Surface mapping of gastric motor functions using MRI: a comparative study between humans and rats". *American Journal of Physiology-Gastrointestinal and Liver Physiology*. 327(3):G345-59, 2024.
- [8] Haldar JP, Setsompop K. "Linear Predictability in MRI Reconstruction: Leveraging Shift-Invariant Fourier Structure for Faster and Better Imaging". *IEEE Signal Processing Magazine*. 37:69-82 2020.
- [9] Lobos RA, Chan CC, Haldar JP. "New theory and faster computations for subspace-based sensitivity map estimation in multichannel MRI". *IEEE Transactions on Medical Imaging*. 43:286-296, 2023.
- [10] Uecker M, Lai P, Murphy MJ, Virtue P, Elad M, Pauly JM, Vasanawala SS, Lustig M. "ESPIRiT—an eigenvalue approach to autocalibrating parallel MRI: where SENSE meets GRAPPA". *Magnetic Resonance in Medicine*. 71:990-1001, 2014.
- [11] Haldar JP, Zhuo J. "P-LORAKS: Low-rank modeling of local k-space neighborhoods with parallel imaging data". *Magnetic Resonance in Medicine*. 75:1499-1514, 2015.

## Figures

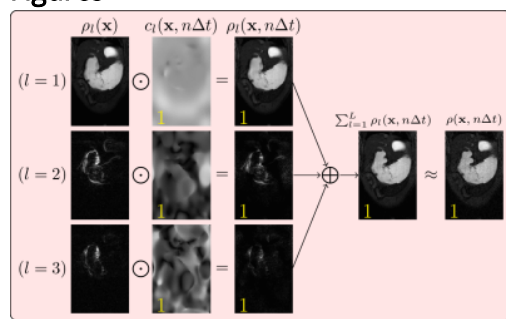


Figure 1. Visual representation of the STM expansion using T1-weighted single-coil gastrointestinal animal Cartesian data acquired as in Wang et al<sup>6</sup>. Only magnitude images of 15/100 time-frames are shown. The fully-sampled data is shown on the very right, which presents a substantial variability of the temporal/spectral characteristics across voxels. Three components were selected for the STM expansion as suggested by the eigenvalue analysis in Fig. 2. For simplicity, we selected the same number of components for each voxel; however, this selection can be made voxel-dependent.

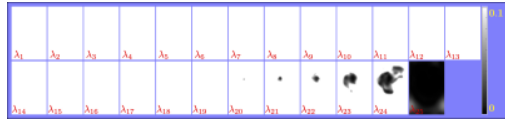


Figure 2. Eigenvalue maps of the  $G(\mathbf{x})$  matrices (sorted in decreasing order) calculated from the data in Fig. 1. The nullspace dimensionality of each matrix (i.e., the number of components in the STM expansion) was estimated as the number of eigenvalues close to zero. We selected this number by counting the eigenvalues below a threshold equal to 0.01. Voxels in stationary areas had a nullspace dimensionality  $L(\mathbf{x}) = 1$ , and voxels in more dynamic areas presented a nullspace dimensionality  $L(\mathbf{x}) \leq 3$ .

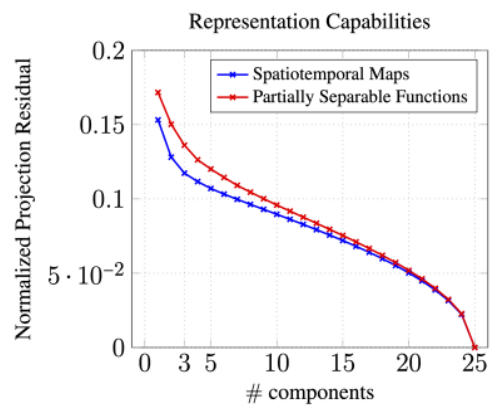


Figure 3. Normalized projection residual (NPR) for the STM and the PSF expansions using the data in Fig. 1 for a varying number of components. NPR corresponds to the NRMSE between the original data and the approximation given by the expansion. STM always obtained a smaller NPR than PSF for a small number of components. Particularly, the NPR obtained by STM using three components (the number used in our reconstruction experiments) was obtained by PSF when using five components. These better representation capabilities (more parsimonious) were also observed qualitatively (not shown).

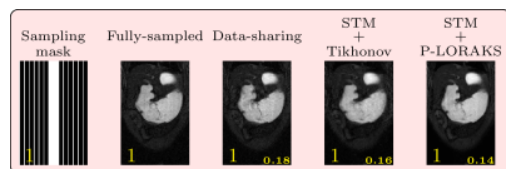


Figure 4. Retrospective reconstruction results using the data in Fig. 1. Only 15/100 time-frames are shown. The sampling mask selects 24/84 phase-encoding lines where 12 vary across time-frames, and 12 are fixed as autocalibration data and used to calculate the STM spatiotemporal functions  $\{c_l(\mathbf{x}, n\Delta t)\}$ . As a baseline, we show a data-sharing reconstruction obtained by constructing a fully-sampled dataset for each time-frame using data from nearby time-frames. We report the NRMSE in each case (bottom-right) considering the total of 100 time-frames.

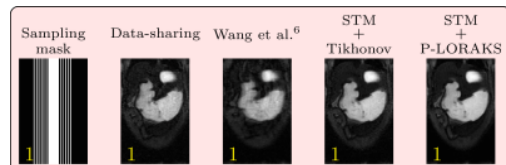


Figure 5. Prospective reconstruction results using data acquired as in Wang et al<sup>6</sup>. 15/100 time-frames are shown. The sampling mask selects 24/48 phase-encoding lines where 12 vary across time-frames, and 12 are fixed as autocalibration data. The reconstruction in each case was performed for a total of 48 phase-encoding lines and zero-padded to match the dimensions in Fig. 4 (84 PE lines). As a comparison, we show reconstruction results using the method in Wang et al<sup>6</sup>, where a GRAPPA-type interpolation is performed for each time-frame using the data from the two adjacent time-frames.